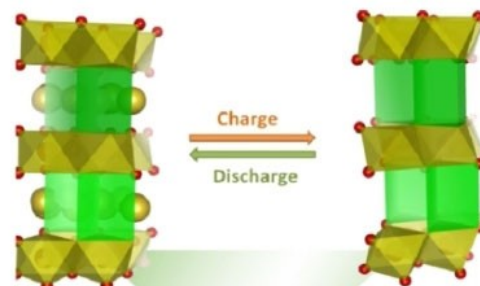


Nickel-Manganese-Based Layered Oxide for Sodium Ion Battery Cathode Materials

Yuheng Gao,^[a] Ping Zhang,^[a] and Renyuan Zhang^{*[a]}



High energy density

Environmentally friendly

Low cost

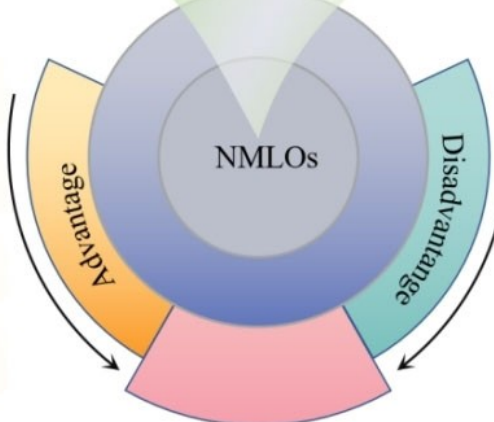
Good Na⁺ conductivity

Phase transition

Poor air stability

Volume expansion

Interface Issues



Sodium-ion batteries (SIBs) have demonstrated significant potential as alternatives to conventional lithium-ion batteries (LIBs) for modern grid and mobile energy storage applications, due to the abundant natural resources and low cost of sodium. Layered transition metal oxides (LTMOs) have attracted much attention due to their high specific capacities, energy densities as well as the compatible preparation processes with those of LIBs cathode materials. Among these, Ni/Mn-based LTMOs

(NMLOs) are particularly noteworthy for their cost-effectiveness and superior electrochemical performance, such as excellent capacity retention, voltage stability, high operating voltage and rate capability. In this review, we briefly introduce the synthesis methods of NMLOs, discuss the challenges, and summarize the solutions. The insights presented may contribute to the development of NMLOs based SIBs.

1. Introduction

SIBs are emerging as a more promising energy storage system for large-scale grid applications, electric vehicles, and renewable energy integration, due to their plentiful availability (the fourth most abundant metal element on earth^[1]), cost-effectiveness, and electrochemical behavior similar to LIBs.^[2-5] However, compared with the smaller diameter size of Li⁺ (0.76 Å), Na⁺ ions, with a diameter of 1.02 Å, can introduce strain in the material lattice and decrease the overall diffusion rate, damaging its structural stability and charge-discharge performance. The performance of SIBs is influenced by the electrode materials, electrolyte, and separator, where the choice of electrode materials is crucial for the effective insertion/extraction of sodium ions, affecting the battery's capacity and cycle stability. Among these components which make up a battery, the cathode material is crucial to the overall performance of the battery. The cathode materials of SIBs can be classified into four types according to their chemical components: layered oxides, organics, Polyanionic compounds, and Prussian blue analogs.^[6] Layered oxide materials have attracted significant attention due to their periodic layered structure, simple preparation methods, and high specific capacity and voltage. They typically feature lower costs and good electrochemical performance. Recent research has been focused on layered oxides due to their remarkable specific capacity, elevated voltage, and simple synthesis techniques.^[7]

LTMOs are generally represented as NaTMO₂, such as: Na_xCoO₂^[8,9] and Na_xMnO₂.^[10-12] TM refers to the transition metal. Generally, the transition metal sites in layered oxides can be occupied by 3d transition metal ions. However, the addition of different 3d transition metal ions results in significant performance differences, making the selection of appropriate 3d transition metal ions very important. Wang et al.^[13] reviewed six different 3d transition metal based layered oxides (NaVO₂, NaCrO₂, NaMnO₂, NaFeO₂, NaCoO₂, and NaNiO₂) electrochemical properties and concluded that Ni-based and Mn-based oxides were appropriate materials for SIBs due to their relatively high battery capacity (NaMnO₂ and NaNiO₂ exhibited battery capacities of 197 mAh/g^[14] and 123 mAh/g,^[15] respectively). However, NaMnO₂ always experiences irreversible phase transition and volume changes caused by Jahn-Teller effect, leading

to substantial capacity decay during the initial charging and discharging process. Ni/Mn-based LTMOs (NMLOs) enable both higher operating voltages due to the redox reactions of Ni and higher specific capacity provided by Mn. In recent years, there have been many works focused on NMLOs, much effort has been paid to enhance the structural stability and electrochemical performance.

In this review, we briefly introduce the various synthesis methods employed for NMLOs, the range of challenges encountered in practical applications, and innovative solutions and optimization strategies designed to address these problems. This article aims to propose promising directions for future research and development of NMLOs, focusing on their potential for industrialization and large-scale application in energy storage systems.

2. Synthesis of NMLOs

The synthesis method of layered oxides is a key to control their structures and electrical properties. The common synthesis methods of NMLOs include solid-state reaction, hydrothermal method, sol-gel method, solution combustion method, and co-precipitation.

2.1. Solid-State Reaction

The Solid-state reaction method is the most commonly used approach for preparing layered oxide structures, which involves the following processes: material selection and proportioning, mixing and grinding, shaping, heat treatment, and post-processing to produce a new solid structure. Key factors include the reaction temperature, the fineness and mixing of raw materials, the atmosphere during heat treatment, and the duration of the heat treatment.^[16,17] Figure 1a shows the synthesis process of MgO-coated Na_{0.67}Ni_{0.33}Mn_{0.67}O₂.^[18] Sodium carbonate, magnesium oxide, nickel oxide, and manganese oxide are mixed by the chemical stoichiometric ratio, then calcined at 900 °C for 12 h to obtain pure NM samples. Many layered electrode materials have been used as an electrode material for SIBs due to their convenience like: Na_{0.9}Mn_{0.60}Ni_{0.35}Mg_{0.05}O₂,^[19] NaNi_{0.35}Fe_{0.2}Mg_{0.05}Mn_{0.4}O₂^[20] Na_{0.85}Li_{0.12}Ni_{0.22}Mn_{0.66}O₂,^[21] and so on. Solid-state reaction method has significant advantages in terms of operation and scalability, it is an effective choice for materials requiring high

[a] Y. Gao, P. Zhang, R. Zhang

Institute of New Energy for Vehicles, School of Materials Science and Engineering, Tongji University, Shanghai 201804, China
E-mail: ryzhang@tongji.edu.cn

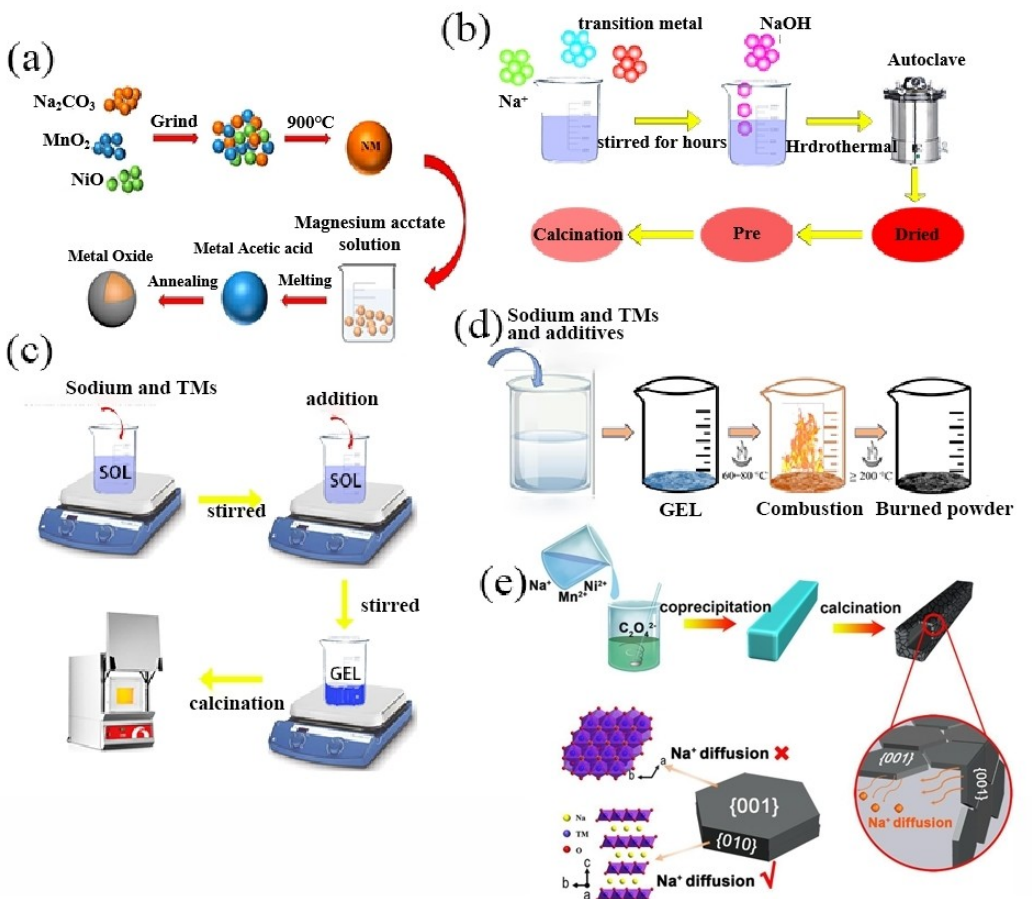


Figure 1. The common synthesis methods of NMLOs: (a) Solid-state reaction method; reproduced with permission from Ref.^[18] Copyright (2024) Frontiers Media S.A.; (b) Hydrothermal method; (c) Sol-gel method; (d) Solution combustion method; (e) Co-precipitation method; reproduced with permission from Ref.^[30] Copyright (2024) Elsevier B.V.

crystallinity and specific morphology. However, it is limited by its inconsistent particle size distribution.



Yuheng Gao is currently pursuing a master's degree at Tongji University. He completed a bachelor's degree at Wuhan University of Technology from 2023. His research focuses on the development of cathode materials for sodium-ion batteries.



Renyuan Zhang received his Ph.D. degree from Fudan University. He is currently a professor at the Institute of New Energy for Vehicles, School of Materials Science and Engineering, Tongji University. His research interest mainly focuses on energy storage materials, mesoporous materials and nano-materials.



Ping Zhang received his BS degree in the Materials Science and Engineering at Hunan University in 2021. He is presently a PhD candidate in the Materials Science and Engineering at Tongji University. His research focuses on materials development for electrochemical energy conversion and storage fields.

2.2. Hydrothermal Method

Hydrothermal synthesis is a method of chemical synthesis conducted under relatively low temperature (100–300 °C) and high pressure conditions (> 1 Mpa), using water as a solvent in a sealed vessel. This method is particularly suitable for synthesizing various inorganic materials, crystals, and some organic-inorganic composite materials (Figure 1b). The key advantage of hydrothermal synthesis is its ability to achieve material synthesis at relatively low temperatures while maintaining high reaction rates and product purity.^[22] Many cathode materials have been prepared through this method like: $\text{Na}_{0.67}\text{Mn}_{0.67}\text{Ni}_{0.22}\text{Co}_{0.07}\text{O}_2$ ^[23] and $\text{Na}_{0.67}\text{Ni}_{0.2}\text{Co}_{0.2}\text{Mn}_{0.6}\text{O}_2$.^[24] In addition, if a different solvent is used instead of water during the synthesis process, it is called a solvothermal method. Compared to hydrothermal methods, solvothermal methods can control the rate, selectivity, and properties of the products by selecting different solvents, thereby achieving control over the morphology, size, and structure of the resulting nanomaterials. Wei et al.^[25] precisely controlled the reaction temperature at 180 °C for 18 hours and successfully synthesized uniform layered vanadium oxide ultrathin nanobelts. Furthermore, the pre-intercalation of iron ions into the vanadium oxide layers significantly suppressed the lattice breathing during sodium ion insertion/extraction. This approach not only tailored the inter-layer spacing but also optimized the material's structure.

2.3. Sol-Gel Method

Sol-gel technology involves the hydrolysis and condensation reactions of chemical precursors in a liquid medium, gradually forming uniformly dispersed nanoparticles (sol), which then aggregate and grow into a continuous three-dimensional network (gel)^[26] (Figure 1c). The particle size, morphology, and chemical composition of the final products can be effectively controlled by fine-tuning the reaction conditions, such as temperature, pH value, and precursor concentration. This technique allows for precise control over the microstructure of the final materials, making it highly applicable in fields such as catalysis, energy, electronics, and biomedical science. The sol-gel method achieves microstructure control through the selection of reactants, sol-gel process, temperature and time regulation, additives, and the adjustment of other parameters. Acetate precursors form plate-like structures, while nitrate precursors form spherical particles. Temperature and time influence the crystal growth rate and crystallinity.^[27] However, it is prone to introducing impurities, and the drying and calcination process may lead to material shrinkage and cracking.

2.4. Solution Combustion Method

The solution combustion method can rapidly synthesize various materials like oxides, ceramics, and composites through the exothermic reaction of metal precursors with organic fuels. This

process (Figure 1d) is efficient. It can save synthesis time and is energy-efficient, producing final products with high purity, uniform particle size distribution, and good sintering characteristics. Moreover, this technique is applicable to a wide range of precursors, making it an ideal choice for producing large quantities of inorganic nanomaterials. Many researchers have used this method to synthesize high-performance cathode materials. The solution combustion method has the advantages of rapid reaction, simple operation, and low cost. Besides, the high-temperature combustion process facilitates the crystallization of materials. However, the combustion and calcination process require high temperature and the combustion process may introduce unburned carbon or other impurities, affecting the purity of the material. Kumar et al.^[28] adopted the solution combustion method to synthesize amorphous $\text{Na}_{0.67}\text{Mn}_{0.5}\text{Fe}_{0.5}\text{O}_2$ within minutes. However, to completely remove the organic impurities, the sample needs further calcination for hours.

2.5. Co-Precipitation Method

Co-precipitation is a widely used wet chemical technique in the synthesis of inorganic materials.^[29] It involves mixing solutions of two or more soluble salts and triggering a chemical reaction under specific conditions to simultaneously precipitate a solid product containing mixed components (Figure 1e).^[30] Its primary advantage lies in the ability to mix different elements at the atomic or molecular level, resulting in precursors for composite materials with uniform chemical composition and good dispersion. The process includes solution preparation, pH adjustment to control the morphology and purity of the precipitate, precipitation formation, filtration and washing of the precipitate to remove possible impurities, and drying and possibly calcining to achieve the desired phase. The significant benefits of the co-precipitation method include its simplicity, scalability for industrial applications, and cost-effectiveness, making it an ideal choice for producing high-performance materials with uniform composition and structure.

In summary, among these five methods, the solid-state reaction method requires a long time and relatively high temperatures. It is relatively simple to operate and results in the highest crystallinity, but the particle size is usually large and uneven. The hydrothermal method generally operates at lower temperatures of 100–300 °C and is more complex to operate because it requires an autoclave. The particle size of the powder typically ranges from 0.1 μm to several micrometers, with high crystallinity. Longer hydrothermal times lead to more pronounced crystallization. The sol-gel method takes a longer time and can be conducted at 500–700 °C. It is easy to control the particle size and shape, resulting in small and uniform particles, but potential pore issues may affect the material's crystallinity. The solution combustion method is very fast, usually completed in a few minutes to a few hours, and the combustion process can reach temperatures above 1000 °C. It requires precise control of the combustion process to achieve small and uniform particles. Despite the short reaction time, the high temperature during combustion helps form highly ordered crystal structures.

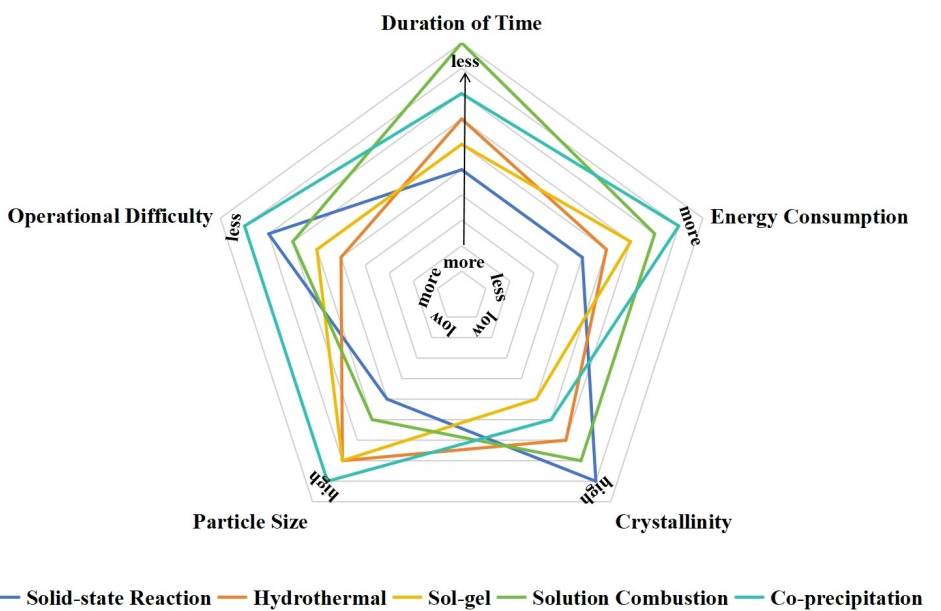


Figure 2. Comparison of Synthesis Methods for Sodium-Ion Battery Cathode Materials.

The co-precipitation method operates at room temperature to 200°C, is simple to operate, and is easy to scale up. It can achieve particle sizes in the tens of nanometers range and has high crystallinity. The characteristics of different synthesis methods are shown in Figure 2.

3. Challenges of Layered Oxides

Although NMLOs offer significant advantages such as high energy density, and high operating voltage, they face substantial challenges including irreversible phase transitions, structural instability, high sensitivity to environmental factors, and side reactions with the electrolyte. These issues impact the performance and stability of NMLOs, posing challenges to their application in the battery sector. In a bid to approach these concerns, strategies like element doping, phase composite strategies, and interface/surface structure control can be employed. These approaches aim to improve the structural stability and enhance the electrochemical performance of NMLOs, thereby advancing their prospects in battery technology.

3.1. Irreversible Phase Changes

Based on the stacking sequence of alkali ions between layers, layered transition metal oxides are typically categorized into O-type and P-type structures according to Delmas.^[31,32] These structures are characterized by edge-sharing MO_6 (Na_xMO_2)^[14] octahedral layers interspersed with Na ions layers, with ionic species inserted into either octahedral (O) or prismatic (P) environments. Symbols O2, O3, P2, and P3 specify the count of

Na ion layers in octahedral or prismatic formations while apostrophe (') symbolizes a monoclinic twist.

P2 and O3 are the most commonly obtained types of the LTMOs (Figure 3). The space group of P2-type layered oxides is typically $\text{P}6_3/\text{mmc}$. The sodium ions migrate through channels (directly from one prismatic site to another) between layers, which supports rapid ion transport. The stacking sequence of this kind of structure is ABAB. This structure allows sodium ions to move under a lower energy barrier and reduce the volume change of the material during charge and discharge processes, which facilitates the intercalation and deintercalation of sodium ions and stabilizes phase structure.^[33] The structure of O3-type layered oxides is constructed based on a face-centered cubic (fcc) array of O^{2-} ions. The stacking sequence of this kind of structure is ABCABC, and sodium ions and transition metal ions are placed at different types of octahedral voids due to their different ionic radius. As the sodium content is high, O3-type

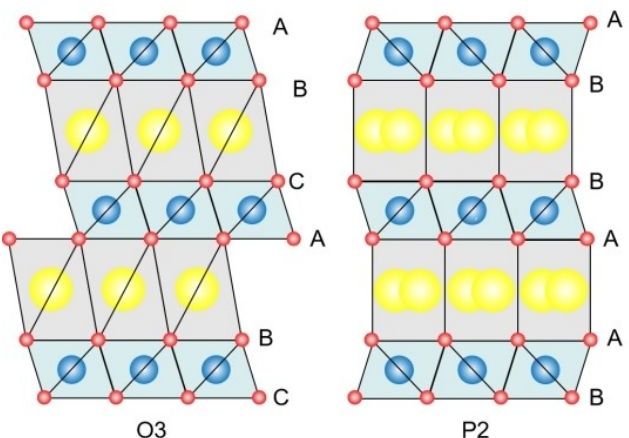
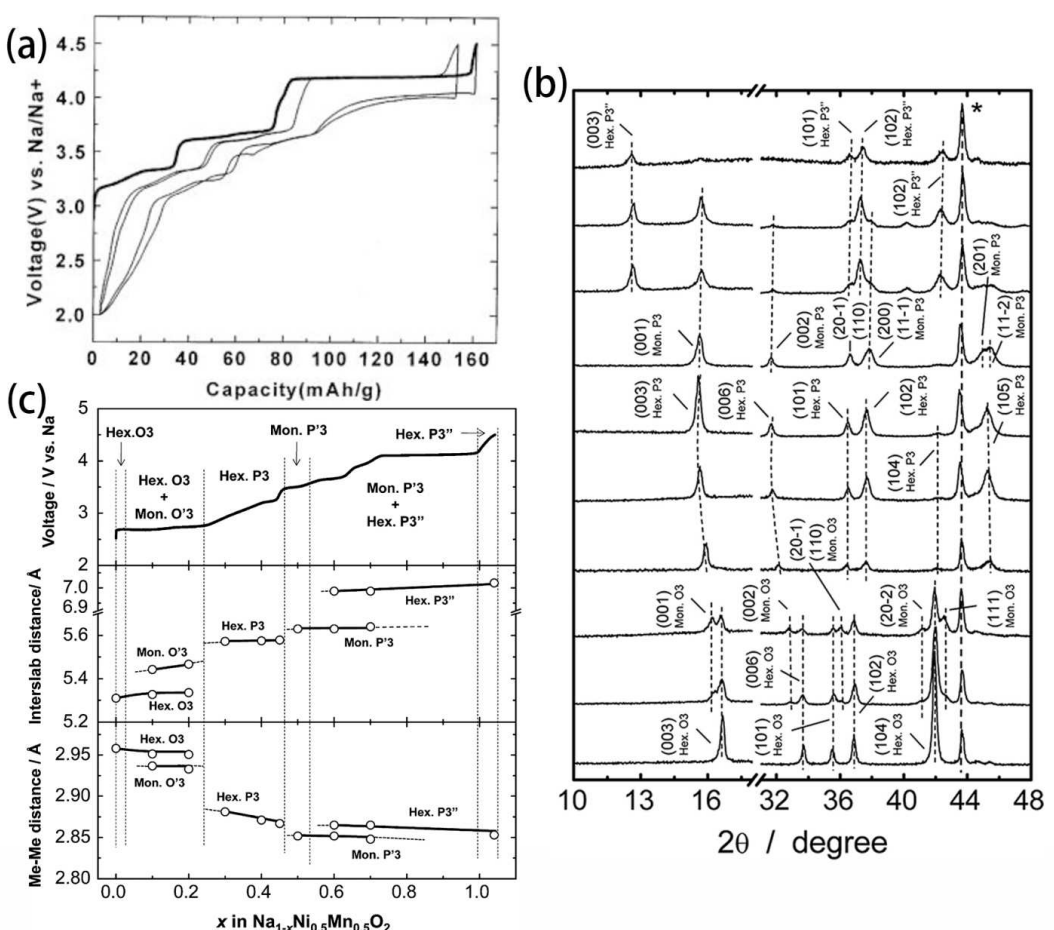


Figure 3. Structure of P2 and O3 phase.

layered oxides have an excellent theoretical capacity and high initial Coulombic efficiency. However, during charging/discharging, the TM_2 layers can undergo displacement without breaking the TM–O bonds, which can easily lead to misalignment between layers under high temperature and pressure conditions, and misalignment between layers can lead to longer or more complex diffusion paths for sodium ions within the electrode material. This increased path length or complexity raises the energy barrier for sodium ion migration, resulting in a slower ion migration rate. The misalignment between layers may compromise the structural integrity of the electrode material, reducing its structural stability. Moreover, the migration path for sodium ions involves moving from an octahedral site to a tetrahedral site before reaching another octahedral site. This process contributes to the suboptimal rate capabilities due to the increased energy barrier and the restricted pathway.^[34]

Both P2 and O3 phases frequently undergo a series of phase changes characterized by variations in the stacking order of their oxide layers. The P2 phase often transfers to the O2 phase due to the sliding of TMO_6 octahedral layers with the elimination of Na^+ during the charging and discharging

process.^[16] This leads to a notable contraction in the crystal structure and a reduction in the distance between layers. The sliding of TMO_6 happens when a certain amount of sodium ions are extracted from the system,^[35] leading to a reorganization of the chemical structure to balance the charge and reduce the overall energy. This reorganization typically involves the $3/2$ rotational sliding of the TMO_6 octahedral layers, aiming to create new octahedral sites for Na^+ and optimize vacancy distribution, thereby achieving a more stable and symmetric structure while minimizing energy. In 2001, Lu et al.^[36] reported that the typical P2-type cathode material $\text{Na}_{2/3}\text{Ni}_{1/3}\text{Mn}_{2/3}\text{O}_2$ presented an apparent plateau above 4.2 V (Figure 4a). The voltage platform near 3.8 V corresponded to the oxidation of Ni^{2+} to Ni^{4+} , while the change in the voltage platform near 4.2 V indicated an irreversible structural phase transition within the material, which can result in a significant volume change of around 20%. This structural change hinders the smooth insertion and extraction of sodium ions, leading to a decrease in capacity and efficiency during repeated cycles. The instability caused by the phase transition also exacerbates the formation of cracks and defects and further reduces the performance and lifespan in practical applications.



A similar issue occurs in the O3-type structure. The O3 phase transition process is usually more complex than that of the P2 structure. During the charging and discharging process of a battery, sodium ions move from the original edge-shared octahedral sites to more stable prismatic sites through the sliding of TMO_2 layers (without breaking the TM–O bonds), leading to a structural reorganization. This process changes the oxygen stacking sequence from “AB CA BC” to “AB BC CA”. Komaba et al.^[37] reported the specific phase transition process of O3-type $\text{NaNi}_{0.5}\text{Mn}_{0.5}\text{O}_2$ via ex situ XRD analysis. Figure 4b and c show that $\text{Na}_{1-x}\text{Ni}_{0.5}\text{Mn}_{0.5}\text{O}_2$ gradually undergoes a phase transition from O3 to O'3 to P3 to P'3 to P3'' and indicate that when $\text{NaNi}_{0.5}\text{Mn}_{0.5}\text{O}_2$ fully transforms into the P3'' phase (4.5 V), the interlayer distance is about 7.0 Å, which potentially embedding solvent molecules in the gaps between the slabs and damaging the overall structure.

In summary, P2 and O3 phases undergo irreversible phase transitions when the voltage exceeds 4.2 V and 4.0 V respectively. Although we can avoid these phase transitions by reducing the voltage to below 4.2/4.0 V, the capacity may decrease significantly. Recently, several methods have been developed to address this issue, such as doping strategy, biphasic strategy, and coating strategy.

3.1.1. Element Doping

Element doping can address the undesired phase transition. Jiang et al.^[38] introduced copper ions into $\text{Na}_{0.6}\text{Ni}_{0.3}\text{Mn}_{0.7}\text{O}_2$ to address the common P2–O2 phase transition and improve the material's cycle stability. The doping of copper increased the interlayer spacing, which improved the migration environment of sodium ions between layers and helped stabilize the insertion and extraction process of sodium ions under high voltage conditions to inhibit the P2–O2 phase transition. The electrode material P2-type $\text{Na}_{0.6}\text{Ni}_{0.2}\text{Mn}_{0.7}\text{Cu}_{0.1}\text{O}_2$ demonstrated a capacity retention rate of 76% after 100 cycles at a current density of 0.1 C, significantly higher than the undoped sample (49%). The (002) peak gradually shifted to low angles during the charging process (Figure 5a), which improved the diffusion dynamics of Na^+ and allowed the battery to exhibit a longer high-voltage plateau in the high voltage region. During the process of discharging from 4.5 V to 2.0 V, the peak returned to its initial state, indicating the high reversibility of the sodiation/desodiation process. SEM images further confirmed that the surface of undoped sample got blurred with the disappearance of typical layered structures as a consequence of P2–O2 phase transition. Due to the similarity of the radius of Mg^{2+} (0.72 Å) and Ni^{2+} (0.69 Å). Feng et al.^[39] reported that Mg^{2+} doping helped more Na^+ stay at the triangular prismatic sites during the charging process to avoid the sliding of TMO_2 sheets (Figure 5b), it inhibited the undesired P2–O2 phase transition. $\text{Na}_{0.67}\text{Ni}_{0.18}\text{Mg}_{0.15}\text{Mn}_{0.67}\text{O}_2$ delivered an initial discharge capacity of 123 mAh/g at a rate of 0.1C within the range of 2.0 to 4.3 V. After 100 cycles at a rate of 0.1C, the capacity retention of the material remained at 92%, which exceeded the undoped sample. Tao et al.^[40] applied Ti^{4+} doping strategy to synthesize

$\text{Na}_{0.67}\text{Ni}_{0.33}\text{Mn}_{0.52}\text{Ti}_{0.15}\text{O}_2$, the CV test indicated that it had a smoother profile compared to $\text{Na}_{0.67}\text{Ni}_{0.33}\text{Mn}_{0.67}\text{O}_2$, especially over 4.2 V, the strong Ti–O bonds within the transition metal layers stabilized the local structure and disrupted the Na^+ vacancy ordering, inhibiting the P2–O2 transition. $\text{Na}_{0.67}\text{Ni}_{0.33}\text{Mn}_{0.52}\text{Ti}_{0.15}\text{O}_2$ demonstrated a reversible capacity of 106.4 mAh/g after 200 cycles, with a capacity retention rate of 88.78% at a low rate of 0.1 C.

Yuan et al.^[41] synthesized Sb-doped O3-type $\text{NaNi}_{0.5}\text{Mn}_{0.5-x}\text{Sb}_x\text{O}_2$ materials. The effect of Sb doping on the crystal structure and phase transitions was investigated in XRD. The results showed that Sb-doped materials effectively suppress O3–O'3 and P'3–O'3 phase transitions during charging and discharging as shown in Figure 5c and d. It can be observed that the undoped NaNM samples underwent a series of phase transitions during the charge-discharge process, including the shift of O3-(003) and O3-(006) peaks to lower angles, accompanied by the appearance of P3-(003) and P'3-(002) XRD peaks. These phase transitions led to structural damage to the material. In Sb-doped NaNMS-1 samples, the peak shifts of the O3 phase were significantly reduced during the charge-discharge process, and no O'3 phase appeared, indicating that Sb doping could suppress these phase transitions and maintain the stability of the crystal structure. Xie et al.^[42] investigated O3- $\text{NaNi}_{1/3}\text{Fe}_{1/3}\text{Mn}_{1/3}\text{O}_2$. Fe doping balanced Ni/Mn ratios and maintained integrity during cycling. At 4.3 V, Ni and Fe oxidized to a tetravalent state, preventing monoclinic transitions (below 4.0 V). Between 3.0–4.3 V, new phases O3' and P3' formed. Above 4.3 V, a stable OP2 phase (Figure 5e) formed with 5.13 Å interlayer spacing, smaller than 5.72 Å of P3'' phase, preventing anion and solvent insertion.^[43] Zhang et al.^[44] reported the doping $\text{Na}_{2/3}\text{Ni}_{1/3}\text{Mn}_{2/3}\text{O}_2$ (NNMO) with Fe to suppress oxygen release and the P2–O2 phase transition. XPS and DEMS revealed that Fe doping could form $\text{Fe}(\text{O}-\text{O})$ species, stabilizing the $\text{O}^{2-}/\text{O}_2^{\text{n}-}$ redox process, and reducing irreversible capacity loss from 25% to 4%. The Fe-doped material exhibits a discharge capacity of 141 mAh/g with 78% capacity retention after 100 cycles.

Although single element doping can suppress irreversible phase transitions, certain element doping may reduce the capacity of the material. Therefore, we can adopt multi-element doping to mitigate this issue. Zhang et al.^[45] reported that Li^+ and Ti^{4+} co-doping can significantly inhibit irreversible P2–O2 phase transition. Ti^{4+} ions can strengthen the lattice structure and reduce crack formation and structural degradation while Li^+ can increase the total capacity of the material by providing additional sodium-ion storage sites. During the charging process, an expanded lattice parameter c and contraction of the ab plane was observed from the *in situ* XRD analysis, which can be attributed to the increasing electrostatic repulsive force between TMO_2 layers and the oxidation of transition metal ions as the Na^+ content decreased. Additionally, when charging to 4.2 V, a new Z phase appeared, which was an intergrowth structure of P-type layers and O-type stacking faults, much closer to the P2 structure with fewer stacking faults compared to the O2 or OP4 phases. Moreover, the P2-Z phase transition showed great reversibility with little volume change of 2.87%,

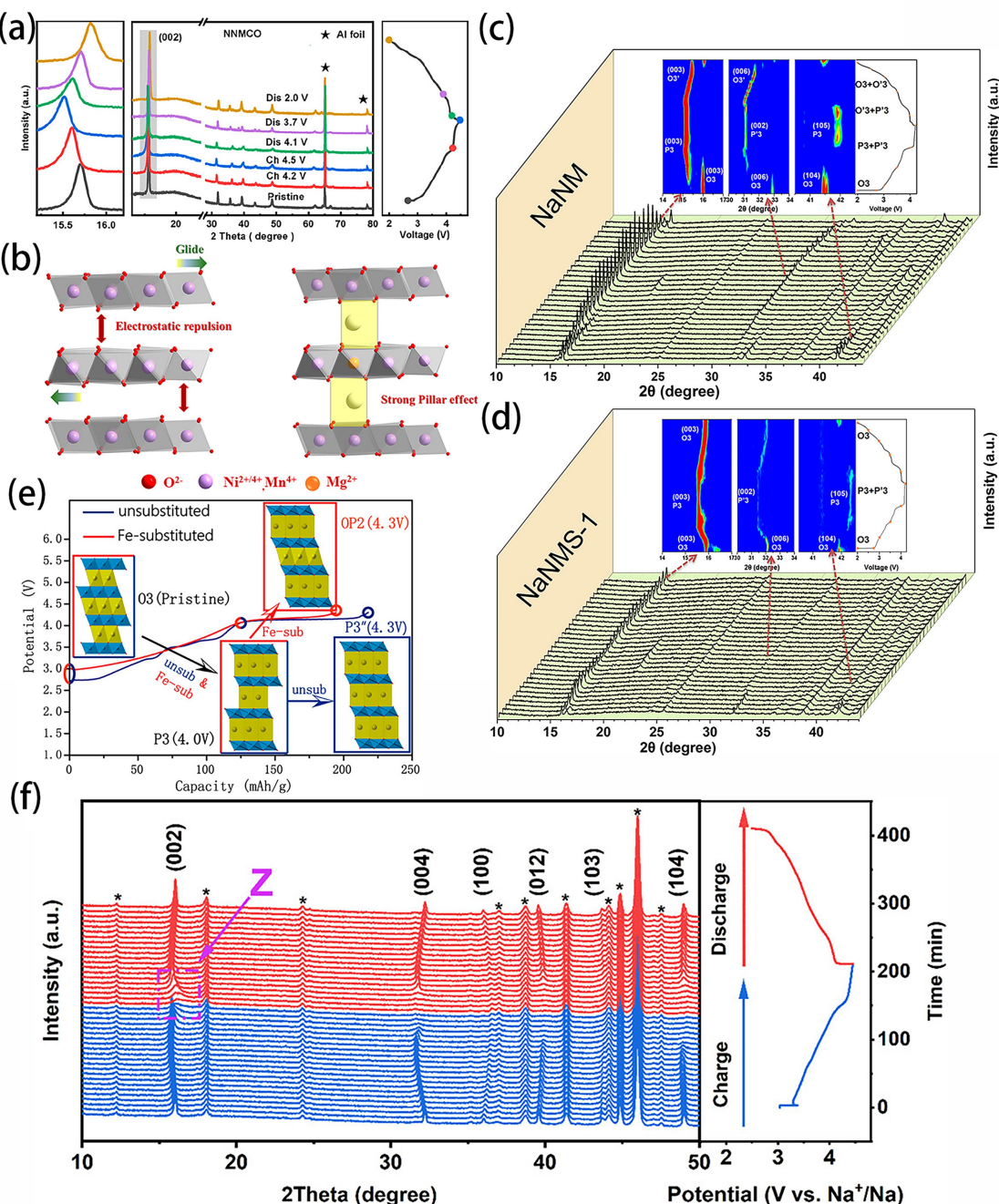


Figure 5. (a) Ex situ XRD patterns of NNMCO at different states of charge; reproduced with permission from Ref.^[38] Copyright (2022) American Chemical Society; (b) Structure simulation of $\text{Na}_{0.67}\text{Ni}_{0.33-x}\text{Mg}_x\text{Mn}_{0.67}\text{O}_2$; reproduced with permission from Ref.^[39] Copyright (2022) American Chemical Society; (c) In situ XRD collected at the first charge/discharge process of the NaNM and (d) NaNMS-1 between 2 and 4.2 V; reproduced with permission from Ref.^[41] Copyright (2022) American Chemical Society; (e) OP2 structure; reproduced with permission from Ref.^[43] Copyright (2015) American Chemical Society; (f) In situ X-ray diffraction patterns of the NNLMTO cathode collected during the first charge/discharge process with a current density of 0.2C; reproduced with permission from Ref.^[45]

indicating that the number of O-type stacking faults was significantly reduced. Wang et al.^[46] reported that $\text{NaNi}_{0.4}\text{Mn}_{0.4}\text{Cu}_{0.1}\text{Ti}_{0.1}\text{O}_2$ demonstrated superior electrochemical performance. As sodium is extracted from the cathode, the (003) peak shifts to a lower angle, and the P3 phase forms. During the discharge process, the P3 phase transformed back to the O3 phase, demonstrating that the O3-P3 phase trans-

formation process is highly reversible. This superior performance is attributed to the synergistic effect of copper and titanium. Titanium doping typically results in an increase in interlayer spacing due to the larger ionic radius. Meanwhile, doping with copper ions can reduce the energy difference between OP phases and provide higher capacity for the system through the redox reactions of copper ions.

Other researches also show the potential advantage of multi-doping strategies, such as Cu/K co-doping^[47] and Cu/Mo co-doping.^[48] It is evident that multi-element doping has better effects compared to single-element doping for P2-type nickel-manganese-based cathode materials. It allows for the optimal selection of dopant ions to specifically target the suppression of the P2–O2 phase transition and to enhance the operating voltage of the material. Element doping can effectively optimize the microstructure of the material and enhance its electrochemical performance under high-voltage conditions by selectively introducing different doping elements. This approach is regarded as a key method for improving the performance of SIB cathode materials.

3.1.2. Coating Strategy

Coating technology is another common method for suppressing irreversible phase transitions. Metal oxides are commonly used as coating materials. Shi et al.^[49] coated the surface of the $\text{Na}_{0.78}\text{Al}_{0.05}\text{Ni}_{0.33}\text{Mn}_{0.60}\text{O}_2$ cathode material with an Al_2O_3 layer. Al_2O_3 coating effectively controls the P2–O2 phase transition at high voltage. It inhibits redox reactions at high voltage and reduces the formation of high-valence manganese and nickel states, thereby preventing irreversible phase transitions. The coating can enhance the specific capacity and rate performance of electrode materials. The $\text{Na}_{0.78}\text{Al}_{0.05}\text{Ni}_{0.33}\text{Mn}_{0.60}\text{O}_2$ material exhibited a high specific capacity of 145.2 mAh/g and a capacity retention rate of 85.1% after 100 cycles. Besides, phase transitions at high voltage lead to gas release. Specifically, the redox reactions in $\text{Na}_{2/3}\text{Ni}_{1/3}\text{Mn}_{2/3}\text{O}_2$ cathode materials involve the oxidation of oxygen anions. This results in the formation of unstable O_2^{n-} species, which can further oxidize to O_2 , leading to oxygen release. Zhang et al.^[50] constructed ultrathin ceria (CeO_{2-x}) heterostructures on $\text{Na}_{2/3}\text{Ni}_{1/3}\text{Mn}_{2/3}\text{O}_2$ (NNM). These nanosheets formed Ce–O–TM bonds, stabilizing lattice oxygen anions and suppressing oxygen release. The NNM/CE-5 cathode retained 75.3% capacity after 100 cycles at 0.5 C. Additionally, many other metal oxides have been applied in coating technologies, such as MgO ,^[51,52] ZrO_2 ,^[53] and ZnO .^[54,55]

Phosphate coatings offer superior ionic conductivity and thermal stability and the incorporation of PO_4^{3-} polyanions into the lattice binds strongly with transition metal cations, reducing the thickness of the transition metal layer and thus promoting greater structural stability due to its high electronegativity.^[56] Tang et al. utilized a $\text{NaTi}_2(\text{PO}_4)_3$ (NTP) surface coating to inhibit phase transitions in P2-type $\text{Na}_{0.67}\text{Ni}_{0.33}\text{Mn}_{0.67}\text{O}_2$ (NMO) cathode materials.^[57] The NTP coating reduced interface impedance and promoted Na^+ diffusion at the interface between the electrode and electrolyte to maintain the material's electrochemical stability. Meanwhile, the NTP coating prevented P2–O2 phase transitions and volume changes during charging/ discharging cycles, reducing crack formation and particle shedding. The NTP-coated sample exhibited excellent electrochemical performance, achieving a capacity retention of 77.4% after 200 cycles and a specific capacity of 106.8 mAh/g at a rate of 5 C.

In summary, compared to element doping, coating technology can further optimize the surface properties of materials. Different metal oxides and phosphate coatings have demonstrated unique advantages in enhancing the performance of NLMOs. Therefore, coating technology is also an effective method for suppressing irreversible phase transitions and improving the cycle stability of electrode materials.

3.1.3. Biphasic Strategy

For most of the P2 type layered oxide, low initial Coulombic efficiency due to the irreversible phase transition is a major challenge.^[58] However, the P3 type belongs to a hexagonal structure, sodium ions have more space between layers, which facilitates the rapid diffusion of sodium ions. Zhou et al. proposed a layered biphasic cathode material $\text{Na}_{0.7}\text{Li}_{0.06}\text{Mg}_{0.06}\text{Ni}_{0.22}\text{Mn}_{0.67}\text{O}_2$ by integrating the characteristics of the P2 and P3 phases.^[59] The cathode delivered highly reversible P2/P3–P2/OP4 structural evolution (Figure 6a). When the electrode was discharged below 4.0 V, the OP4/P3 phase reverted to the P2/P3 structure, as the OP4/P3 phase transition was more reversible compared to that of O2/P3. Therefore, it provided a reversible capacity of 119 mAh/g and an excellent rate performance with 85.5% capacity retention at 5 C. The migration speed of sodium ions can be improved by precisely controlling the ratio and distribution of the P2 and P3 phases. This optimization enables the composite phase materials to maintain a high specific capacity and good capacity retention under high-rate discharge conditions.

As mentioned above, P2 and O3 are the two most common phase structures in layered oxides and each of them suffers from irreversible phase transitions. Interestingly, by combining the P2 and O3 phases, the material can both achieve high capacity and deliver enhanced cycle stability. Besides, Constructing the P2/O3 composite structure can achieve the highly reversible phase transition process of P2/O3–P2/P3–OP4/OP2.^[60] Hu et al. used a simple solid-state method to synthesize 4 types of P2/O3 biphasic layered oxides (Figure 6b).^[61] All of the P2/O3 biphasic layered oxides exhibited specific capacities exceeding 120 mAh/g. The P2 phase provides rapid ion transport channels, while the O3 phase offers high energy storage capacity. This biphasic structure better maintains the integrity of the crystal structure during the insertion and extraction of sodium ions, reducing lattice stress during high-rate charging and discharging, thus improving the material's cycle stability and rate performance. However, it has been challenging to regulate accurately the phase ratio of P2/O3 composite due to their high compositional diversity, which presents an important research topic for future researchers.

Although P2/O3 biphasic strategy can integrate the advantages of both P2 and O3 phases. P2 type cathode materials may undergo a P2–O2 phase transition more or less, while P3 phase has a slightly larger interlayer spacing and a larger trigonal superlattice structure which is described in Figure 6c. For example, P3-type $\text{Na}_{0.67}\text{Ni}_{0.5}\text{Mn}_{0.5}\text{O}_2$ has better structural stability compared to P2-type $\text{Na}_{0.67}\text{Ni}_{0.5}\text{Mn}_{0.5}\text{O}_2$,^[62] which helps maintain

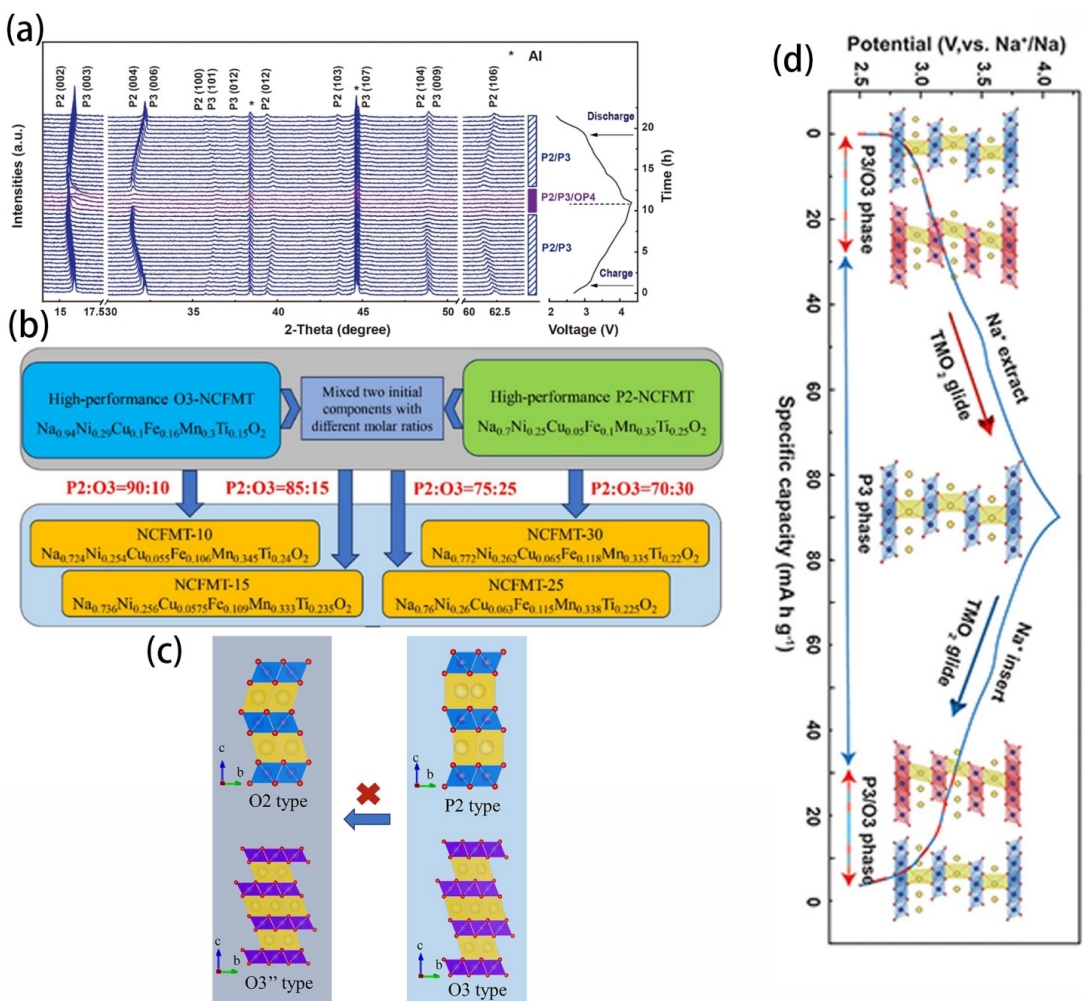


Figure 6. (a) Evolution of the electrochemical behavior of P2/P3-NLMNM compounds during the first charge/discharge; reproduced with permission from Ref.^[59] Copyright (2018) Elsevier Ltd; (b) Electrochemical performance comparison of P2/O3 NCFMT layered oxide cathode materials with different molar ratios; reproduced with permission from Ref.^[61] Copyright (2023) American Chemical Society; (c) Diagram of Unfavorable Phase Transitions in P2/O3 Phases; reproduced with permission from Ref.^[61] Copyright (2023) American Chemical Society; (d) Crystal structure evolution of P3/O3-NNMT at different charged/discharge states; reproduced with permission from Ref.^[63] Copyright (2021) Wiley-VCH GmbH.

the integrity of the electrode material during long-term cycling and reduces capacity degradation. Additionally, the P3 phase can remain stable over a wider range of potentials, meaning that P3 phase materials can operate at higher or lower voltages, increasing their applicability in various applications. Besides, the P3 phase shares some similarities with O3 phase in structure, which means P3 phase can transfer to O3 phase more easily compared to P2 phase. Zhang et al.^[63] successfully prepared the P3/O3 composite phase $\text{Na}_{2/3}\text{Ni}_{1/3}\text{Mn}_{2/3}\text{O}_2$ biphasic cathode material for SIBs through the substitution of Ti^{4+} for Mn^{4+} by using the sol-gel method, the P3/O3 composite phase cathode material exhibited excellent rate capability and cycling stability, outperforming the single-phase P3 and O3 materials. The crystal structure evolution of P3/O3-NNMT is shown in Figure 6d. It maintained 88.7% of its initial capacity at a high rate and retained 68.7% of its capacity after 2000 cycles at 1 C. Other researchers successfully synthesized P3/O3 biphasic $\text{Na}_{0.9}\text{Fe}_{0.5}\text{Mn}_{0.45}\text{Ni}_{0.05}\text{O}_2$ through solid-state reaction with nickel doping, which exhibited exceptional rate performance and

cycling stability. At a rate of 3 C, the discharge capacity of P3/O3 NFNM was twice more than that of P3/O3 NFM (undoped type). Additionally, the addition of Ni can maintain the P3 phase, thereby improving the electrochemical performance.^[64] In summary, the combination of P3 and O3 phases enhances the material's structural stability. The P3 phase offers larger interlayer spacing facilitating rapid sodium ion diffusion, while the O3 phase provides higher initial specific capacity and energy density. This complementary structure ensures greater stability during cycling, particularly under high-rate charging and extensive cycling conditions. The P3/O3 composite facilitates effective charge transfer and rapid sodium ion diffusion, which is crucial for improving the battery's power output and response speed. Optimizing the composite phase structure provides better ion diffusion paths and lower resistance. These factors collectively contribute to the superior electrochemical performance of P3/O3 composite materials in sodium-ion batteries, making them particularly suitable for applications requiring high energy density and stable cycling performance.

Above all, the biphasic strategy can provide more optimized sodium ion diffusion pathways and higher charge transfer efficiency, while also balancing the material's capacity and stability. This approach demonstrates significant advantages in enhancing electrochemical performance, particularly excelling under high energy density and rigorous cycling conditions, and it is capable of maintaining the structural integrity and electrochemical activity of the material across a wide voltage range.

3.2. Air Instability

Typically, after the calcination of the LTMO materials, the surface of the sample will change from black to other colors (depending on the composition of the electrode materials) and cracks due to volume changes if they are not immediately transferred to a drying chamber for further processing. This is because they have hygroscopic properties upon exposure to air, which can lead to some irreversible physical and chemical changes. The mainstream explanations mainly include three types: (1) The open structure of the layered oxides provides channels for water molecules to penetrate into the interior of the material, allowing water molecules to intercalate within the spaces between layers or to adsorb on the material's surface. The presence of moisture can lead to electrolyte decomposition, corrosion of active materials, or undesirable side reactions (especially when sodium content is high^[37]), causing the deterioration of electrochemical performance. (2) The moisture in the air can chemically extract Na⁺ ions from the sodium layers, forming a protonated phase after Na⁺ is replaced by H⁺. This transformation redistributes the charges within the material because the removal of Na⁺ ions diminishes their shielding effect on the charges between adjacent oxide layers. The removal of Na⁺ leads to a decrease in the shielding effect, thereby increasing the repulsive force between charges of neighboring oxide layers, which in turn enlarges the distance between layers. This structural adjustment could disrupt the material's electrochemical performance, as changes in the interlayer distance affect the efficiency of ion migration within the material.^[65] (3) Layered oxides are capable of capturing CO₂ from the atmosphere, through a novel process at room temperature, as the CO₃²⁻ ions can be intercalated into the transition metal layers. To address these issues, researchers have employed coating techniques and selected appropriate dopants to suppress the side reactions between the electrodes and both air and electrolyte.

3.2.1. Coating Strategy

Surface coating functions as a protective barrier to shield the cathode material from exposure to humid air and helps prevent detrimental side interactions with the organic electrolyte.^[56] Yuan et al.^[66] introduced potassium ions and phosphates to form a mixed coating that enhances the electrochemical performance of NMLOs. Surface reorganization and mixed coating protection. The introduction of potassium ions induced

the rearrangement of surface atoms, forming a birnessite-type K₂Mn₄O₈ structure. This reorganization not only stabilized the surface structure of the material but also reduced reactions with moisture in the air. Meanwhile, the combination with phosphate forms a mixed coating that effectively protects the cathode material from moisture and prevents metal dissolution into the electrolyte. This coating acts as a physical barrier, reducing direct contact of the material with moisture and oxygen. The NKMNO@KM/KP||Na half-cell demonstrated an excellent rate performance at 50 C and maintained 90.1% of its capacity after 100 cycles at 5 C. Furthermore, the NKMNO@KM/KP||HC full cell achieved an energy density of 213.9 Wh/kg.

3.2.2. Doping Strategy

Just like inhibiting phase transitions, the air stability of materials can be enhanced through elemental doping. Cai et al. synthesized an air and moisture-resistant cathode material Na_{0.72}Li_{0.16}Ni_{0.12}Ti_{0.1}Mn_{0.62}O₂ by additionally doping Li and Ti into an NMLO.^[67] Ti⁴⁺ plays a key role in enhancing air stability by strengthening Ti–O bonds and finely tuning energy levels, thereby improving the material's corrosion resistance. This allowed the electrode material to maintain its performance even when exposed to moist and airy environments. Zhang et al. reported that by introducing lithium to replace nickel, the Na_{2/3}Li_{1/9}Ni_{5/18}Mn_{2/3}O₂ (NLNM) material demonstrated excellent water stability and electrochemical performance.^[68] Specifically, density functional theory calculations revealed that Li/Mn units exhibited higher adsorption energy (Figure 7b), making them less susceptible to water adsorption, thus providing better water stability. The NLNM material demonstrated a capacity retention of 78% at high rates and maintained 87% of its capacity after 1000 cycles. These findings indicate that optimizing the composition of the metal layer can significantly enhance the water stability and electrochemical performance of layered oxide cathode materials.

3.2.3. Honeycomb Layered Structure Design

Honeycomb Layered structure (HLO) is a special type of layered oxide structure. Researchers have confirmed that when transition metal elements and heavy metal elements are mixed at a molar ratio of 2:1, a highly ordered and extensible honeycomb network framework tends to form.^[69] The crystal structure is plotted in Figure 7d,^[70] common chemical compositions of it are indicated as Na₃⁺M₂²⁺D₅⁺O₆²⁻.^[71] M represents transition metal ions, and D represents heavy metal ions. Transition metal site ions and heavy metal site ions are both located in the transition metal layers and are arranged in a 2D honeycomb network structure in an orderly manner. This structure can generate high redox potentials and cycling stability at two ionic sites. Transition metals usually function as redox-active centers providing charge and discharge capacity and heavy metals can help to stabilize the structure and prevent irreversible structure change, thus enhancing the whole electrochemical properties.

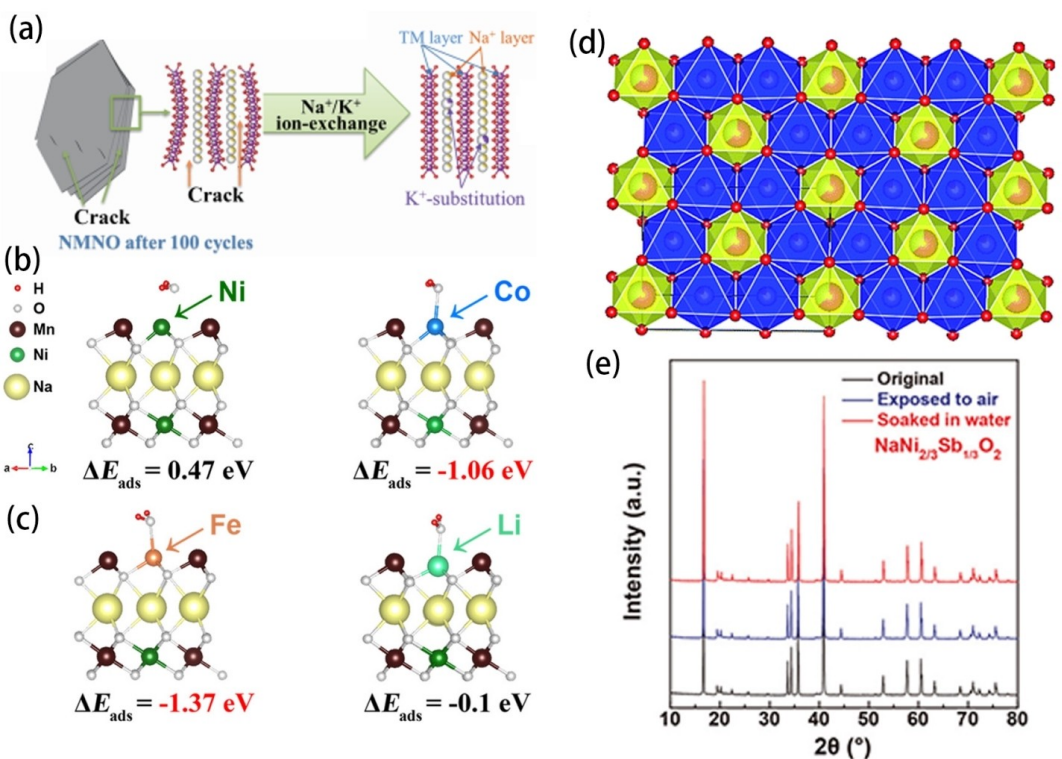


Figure 7. (a) Schematic diagram of the mechanism of K⁺ doping inhibiting particle cracking; reproduced with permission from Ref.^[66] Copyright (2024) American Chemical Society; (b, c) DFT calculated ΔE_{ads} value for Ni/Mn, Co/Mn, Fe/Mn, and Li/Mn units. Reproduced with permission from Ref.^[68] Copyright (2020) American Chemical Society; (d) The crystal structure of honeycomb layered structure. Reproduced with permission from Ref.^[70] Copyright (2017) The Royal Society of Chemistry; (e) XRD patterns of as-synthesized and aged NaNi_{2/3}Sb_{1/3}O₂ sample. Reproduced with permission from Ref.^[72] Copyright (2020) American Chemical Society.

Wang et al. developed a Na₃Ni₂SbO₆ material with a hexa-Ni ring superstructure to explore its role in enhancing air stability.^[72] The Na₃Ni₂SbO₆ was formed by substituting part of the Ni with Sb to create a highly ordered superstructure within the transition metal layers. The stability of this structure primarily stemmed from the orderly arrangement of Ni and Sb. Even after prolonged exposure to air or immersion in water followed by drying, its characteristic diffraction peaks remained unchanged, demonstrating significant抗氧化 and hydrolysis resistance (Figure 7e). However, HLOs with single transition metal (Ni) site ions tend to undergo an O₃–P₃–O₁ phase transition.^[71] So, researchers adopt other ions to construct binary transition metal site ions to limit the volume change and gain better electrochemical performance. Dsoke et al. improved the electrochemical properties of Na₃Ni₂BiO₆ by doping Ti⁴⁺.^[73] The tests showed that doped samples had a more stable voltage platform during charging and discharging and a smoother curve under 1 C for the first and 100th cycles. The introduction of titanium ions reduces the imbalance between Ni and Bi and forms a more stable phase interface to inhibit the phase transition. This change facilitates the rapid diffusion and migration of Na⁺ ions within the honeycomb structure. However, honeycomb-layered oxides also face some electrochemical challenges that the presence of too many inert atoms involved in oxidation-reduction processes leads to low theoret-

ical capacity and there are still many unexplored ion combinations in the transition metal layers that need further research.

In conclusion, HLOs hold significant potential for enhancing the electrochemical performance of electrode materials. By introducing different ion combinations and constructing binary transition metal site ions, its structural stability and sodium ion diffusion pathways can be further optimized. However, due to the presence of many inert atoms involved in redox processes, the theoretical capacity of HLOs remains low, and the ion combinations within the transition metal layers still require further research and exploration.

3.3. Interface Issues

Interface issues between the electrode and the electrolyte during battery operation can lead to capacity loss, structural deterioration, and safety hazards.^[74] The interface stability of NMLOs is closely related to the redox reactions of cations and anions. At higher voltages, oxidized oxygen anions react with the electrolyte. This process can make the electrolyte decompose and the generation of gases that may cause swelling or rupture of the battery casing. Additionally, this process can also create a layer of resistive products on the cathode surface, further impeding ion transfer and degrading battery performance. At lower voltages, low-valence transition metal ions tend

to dissolve into the electrolyte, compromising the stability of the cathode surface structure.^[75] This dissolution process not only reduces the structural integrity of the electrode but also depletes the active material necessary for battery operation, thereby diminishing the overall capacity and longevity of the battery. Lin et al.^[76] detected the reduction of Mn valence and loss of oxygen due to the oxidative decomposition of the electrolyte and observed significant oxygen loss around the nanocracks at the edges of the original particles which led to the reduction and dissolution of transition metal ions. Furthermore, in the subsequent electrochemical processes, adverse reactions between the cathode material and the electrolyte gradually intensified.

3.3.1. Inhibiting the Dissolution of Transition Metal

The dissolution of TM ions happens when the cathode's oxygen oxidizes the electrolyte and this reaction leads to the reconstruction of the cathode surface. During the reconstruction process, the dissolution of TM is exacerbated, creating a vicious cycle. As the reconstruction produces more new surfaces, adverse reactions also increase. So, in a bid to end this vicious cycle, the dissolution of the TM must be inhibited. Ji et al.^[77] used the ALD method to apply an Al_2O_3 coating on $\text{Na}_{2/3}\text{Ni}_{1/3}\text{Mn}_{2/3}\text{O}_2$ to suppress transition metal dissolution. The coating blocked direct contact between harmful substances in the electrolyte and the cathode material. NiF_2 and MnF_2 signals were not obvious, while AlF_3 was easily observed due to the reaction of Al_2O_3 with HF (Figure 8a). The Al_2O_3 coating prevented side reactions controlled the dissolution of metal ions and maintained electrode structure. The CEI film was smooth and resistant to cracking (Figure 8b). The Al_2O_3 -coated

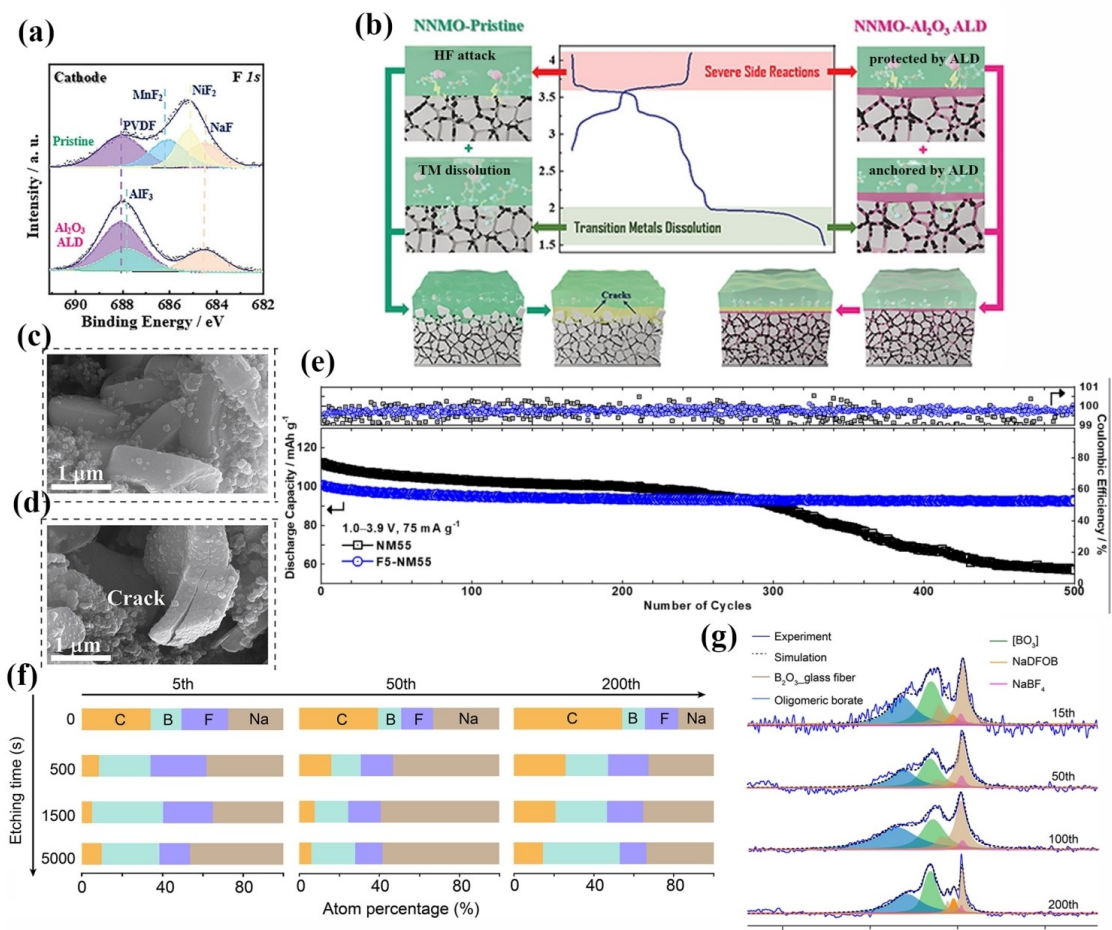


Figure 8. (a) F 1s XPS spectra collected from the cathodes of cycled NNMO-Pristine and NNMO-Al₂O₃ ALD; reproduced with permission from Ref.^[77] Copyright (2021) Wiley-VCH GmbH; (b) Schematic diagram of the failure process at different voltage ranges of the NNMO-Pristine cathode electrode and the protective effect of the Al₂O₃ ALD coating; reproduced with permission from Ref.^[77] Copyright (2021) Wiley-VCH GmbH; (c) SEM images of NNZMTO with 0.1 wt % LiPO₄F₂ and (d) SEM images of NNZMTO without LiPO₄F₂; reproduced with permission from Ref.^[78] Copyright (2023) Science Press and Dalian Institute of Chemical Physics, Chinese Academy of Sciences; (e) Long-term cycling performance of full cells; reproduced with permission from Ref.^[79] Copyright (2024) Royal Society of Chemistry; (f) Atomic percentage of carbon (C), boron (B), fluorine (F), and sodium (Na) in electrodes of various deposition cycles (5th, 50th, and 200th). The results were obtained from XPS depth profiling with different Ar ion etching times. B.E. is binding energy; reproduced with permission from Ref.^[82] Copyright (2024) American Association for the Advancement of Science; and (g) ¹¹B solid-state NMR spectra of SEI species harvested from the Na metal surface after the 15th, 50th, 100th, and 200th cycles; reproduced with permission from Ref.^[82] Copyright (2024) American Association for the Advancement of Science.

electrode exhibited a capacity retention rate of 88.90% after 100 cycles at 1 C and 87% at 5 C, significantly higher than the uncoated electrode. Sun et al.^[78] used LiPO₂F₂ as an electrolyte additive and applied atomic layer deposition technology to form a uniform and ultrathin cathode-electrolyte interphase (CEI) on the surface of Na_{0.67}Ni_{0.28}Zn_{0.05}Mn_{0.62}Ti_{0.05}O₂. This CEI layer effectively blocked the corrosion of the cathode material by the electrolyte and reduced the chemical decomposition and dissolution of transition metals. Figure 8c shows the microstructure of the coated surface, and compared to Figure 8d, it is evident that no crack is formed on the surface. Electrochemical test results showed that with the addition of 0.3 wt % LiPO₂F₂, the NNZMTO electrode exhibited an excellent capacity retention rate of 94.44% after 500 cycles at a current density of 1 C. These physical stresses can cause the material to fracture, thereby increasing the surface area of the cathode material exposed to the electrolyte and making it more susceptible to chemical reactions. These reactions typically result in the decomposition of surface-active substances and the dissolution of transition metal ions. To address this problem, Sun et al.^[79] developed a fluorination strategy by introducing fluorine into the Na[Ni_{0.5}Mn_{0.5}]O₂ material to replace some oxygen, forming more stable metal-fluorine bonds. This approach serves two main purposes: it reduces the formation of microcracks and effectively minimizes the dissolution of transition metal ions while also inhibiting the formation of a NiO-like rock salt phase that can lead to capacity decline. The optimized Na_{0.95}[Ni_{0.5}Mn_{0.5}]O_{1.95}F_{0.05} cathode exhibited excellent cycling stability and displayed at least 133 mAh/g initial capacity under the rate of 0.1 C, and a pouch-type full cell with a hard carbon anode maintained 92% capacity retention after 500 cycles as shown in the Figure 8e.

3.3.2. Adding Electrolyte Additives

In recent years, non-aqueous electrolytes composed of organic solvents, sodium salts, and additives have been a primary focus of research and application. Among these components, additives play a crucial role. Additives can participate in electrochemical reactions at the electrode/electrolyte interface, forming stable solid electrolyte interphase (SEI)/cathode electrolyte interphase (CEI) layers on the electrode surface to enhance the battery's cycling performance, rate capability, and Coulombic efficiency even in a small amount.^[80] Sun et al.^[81] combined succinic anhydride (SA) with fluoroethylene carbonate (FEC) and found that this dual-additive significantly could enhance the battery life of Na_{0.6}Li_{0.15}Ni_{0.15}Mn_{0.55}Cu_{0.15}O₂ cathode materials. After 400 cycles, the capacity retention rate reached 87.2%. The synergistic effect of SA and FEC was primarily realized through the formation of more uniform and stable electrolyte interface layers (CEI/SEI) on the electrode surfaces. SA, with its higher HOMO value, preferentially oxidizes within the high voltage range of the electrochemical window, forming a CEI layer on the cathode surface, while FEC forms an SEI layer on the anode surface. These layers effectively block further decomposition of the electrolyte and excessive deposition of sodium ions, thus

improving the structural integrity and electrochemical performance of the battery. Gao et al.^[82] studied the protective effect of the electrolyte component sodium (NaDFOB) in sodium-ion batteries on the SEI and its mechanism affecting battery performance. The study found that the NaDFOB anion is reduced first in the electrolyte, aiding in SEI formation and suppressing the decomposition of carbonate solvents. Through in-depth analysis using XPS and solid-state NMR as shown in Figure 8f and g, the chemical changes in the SEI during electrochemical cycling were revealed, showing that the anion gradually transforms into a borate- and fluoride-rich SEI. Electrochemical test results indicated that the formed SEI effectively enhances the battery's cycling stability and prolongs its lifespan. Notably, the SEI formed after 50 cycles achieved the optimal chemical composition, extending the lifespan of the SMB by three times. Additionally, the SEI exhibited excellent resistance to electrolyte decomposition, maintaining low electrolyte consumption during cycling, and ensuring long-term stable operation of the battery.

By employing strategies such as surface coating and introducing electrolyte additives, the dissolution of transition metal ions and the structural reconstruction of electrode materials can be effectively suppressed, thereby enhancing the cycle stability and capacity retention of sodium-ion batteries. These methods not only improve electrochemical performance but also extend the battery's lifespan, providing crucial technological support for the development of high-efficiency energy storage systems.

4. Summary and Outlook

The application of NMLOs in SIBs has garnered widespread attention due to their excellent electrochemical performance, particularly in terms of high energy density and cycle stability. Through elemental doping, surface coating, and advanced synthesis methods, researchers have made significant progress in stabilizing NMLOs' structures and suppressing detrimental phase transitions. However, to further advance SIBs towards practical applications, future research must focus on several key areas.

Firstly, an important direction for future research is the continued optimization of NMLOs' microstructure. This includes further improving grain boundaries, reducing particle size, and optimizing the uniform distribution of dopant elements within the material. These improvements will not only enhance the electrochemical performance of the material but also help suppress phase transitions and structural degradation, thereby extending the battery's lifespan.

Secondly, NMLOs' performance in resisting moisture and air oxidation directly impacts their lifespan and safety in practical use. Therefore, future research should focus on developing more corrosion-resistant coating technologies or more stable doping systems to effectively prevent material degradation in humid environments. Moreover, reducing the production costs of NMLOs is crucial for their commercial adoption. By using cheaper and more abundant raw materials, as well as develop-

ing more efficient synthesis processes, the manufacturing costs of these materials can be significantly lowered, increasing their market competitiveness. On this basis, developing scalable manufacturing technologies and effectively integrating NMLOs into complete battery systems will also become important directions for future research.

Thirdly, the focus of SIBs should not be limited to basic research and the performance evaluation of coin cells in the laboratory, since coin cells cannot accurately reflect the performance of commercial pouch cells, as their higher impedance affects cycling stability and rate performance. Additionally, electrolyte additives that are effective in coin cells may not exhibit the same advantages in pouch cells. Future research should shift from coin cells to pouch cells, optimizing the effectiveness of electrolyte additives, enhancing the compatibility between electrodes and electrolytes, ensuring long-term stability under high voltage and high-temperature conditions, and developing scalable manufacturing technologies to promote the large-scale commercialization of SIBs.

Overall, the ongoing research and development of NMLOs in sodium-ion batteries demonstrate their broad prospects in the energy storage field. With the continuous advancement of technology and the expansion of application areas, NMLOs are expected to play a more important role in future energy systems, especially in scenarios that require high performance and safety assurance.

Acknowledgements

This work was funded by the National Natural Science Foundation of China (Grant No. 22279092).

Conflict of Interests

The authors declare no conflict of interest.

Keywords: Sodium-ion batteries • Nickel-manganese-based layered oxides • Elemental doping • Structural stability • Air stability

- [1] E. De La Llave, V. Borgel, K. J. Park, J. Y. Hwang, Y. K. Sun, P. Hartmann, F. F. Chesneau, D. Aurbach, *ACS Appl. Mater. Interfaces* **2016**, *8*, 1867–75.
- [2] M. D. Slater, D. Kim, E. Lee, C. S. Johnson, *Adv. Funct. Mater.* **2013**, *23*, 947–958.
- [3] Y. Sun, S. H. Guo, H. S. Zhou, *Adv. Energy Mater.* **2019**, *9*, 1800212.
- [4] Y. Huang, Y. Zheng, X. Li, F. Adams, W. Luo, Y. Huang, L. Hu, *ACS Energy Lett.* **2018**, *3*, 1604–1612.
- [5] Y. Li, Y. S. Hu, X. Qi, X. H. Li, X. Huang, L. Chen, *Energy Storage Mater.* **2016**, *5*, 191–197.
- [6] J. Y. Hwang, S. Myung, Y. K. Sun, *J. Chem. Soc. Rev.* **2017**, *46*, 3529–3614.
- [7] P. F. Wang, Y. You, Y. X. Yin, Y. G. Guo, *Adv. Energy. Mater.* **2018**, *8*, 1701912.
- [8] X. H. Zhao, H. Wang, S. F. Wang, H. Zhang, J. Wang, G. Fu, *J. Nanosci. Nanotechnol. Lett.* **2014**, *6*, 918–921.
- [9] J. Molenda, D. Baster, A. Milewska, K. Świerczek, D. K. Bora, B. Artur, T. Janusz, *J. Solid State Ionics* **2015**, *271*, 15–27.
- [10] T. Shimono, D. Tanabe, W. Kobayashi, Y. Muritomo, *J. Phys. Soc. Japan* **2013**, *82*, 083601.
- [11] T. Shibata, W. Kobayashi, Y. Moritomo, *Appl. Phys.* **2014**, *7*, 067101.
- [12] N. Bucher, S. Hartung, A. Nagasubramanian, Y. L. Cheah, H. E. Hoster, S. Madhavi, *ACS Appl. Mater. Interfaces* **2014**, *6*(11), 8059–65.
- [13] S. H. Wang, C. L. Sun, N. Wang, Q. C. Zhang, *J. Mater. Chem. A* **2019**, *7*, 10138–10158.
- [14] N. Yabuuchi, R. Hara, K. Kubota, J. Paulsen, S. Kumakura, *J. Mater. Chem. A* **2014**, *2*, 16851–16855.
- [15] M. Sathiya, K. Hemalatha, K. Ramesha, J. M. Tarascon, A. S. Prakash, *Chem. Mater.* **2012**, *24*, 1846–1853.
- [16] Y. Gupta, P. Siwatch, R. Karwasra, K. Sharma, S. K. Tripathi, *Renew. Sustain. Energy Rev.* **2024**, *192*, 114167.
- [17] A. Buekenhoudt, A. V. Kovalevsky, J. Luyten, F. Snijkers, *C. Basic Aspects in Inorganic Membrane Preparation*, **2010**.
- [18] L. Xue, S. Bao, L. Yan, Y. Zhang, J. L. Lu, Y. S. Yin, *Front. Energy Res.* **2022**, *10*, 847818.
- [19] K. Mathiyalagan, K. Karuppiah, A. Ponnapiah, S. Rengapillai, S. Marimuthu, *J. Int. J. Energy Res.* **2022**, *46*, 10656–10667.
- [20] X. Y. Zhang, Y. N. Zhou, L. Z. Yu, S. Y. Zhang, X. X. Xing, W. L. Wang, S. L. Xu, *Mater. Chem. Front.* **2021**, *5*, 5344–5350.
- [21] T. Jin, P. F. Wang, Q. C. Wang, K. J. Zhu, T. Deng, J. X. Zhang, W. Zhang, X. Q. Yang, L. F. Jiao, C. S. Wang, *Angew. Chem. Int. Edn* **2020**, *59*, 14511–14516.
- [22] A. T. Ta, V. N. Nguyen, T. T. O. Nguyen, H. C. Le, D. T. Le, T. C. Dang, *Ceram. Int.* **2019**, *45*, 17023–17028.
- [23] F. Fu, X. Fu, *Solid State Ionics* **2020**, *346*, 115211.
- [24] X. Wang, X. Yin, X. Feng, Y. Li, X. Dong, *Chem. Eng. J.* **2022**, *428*, 130990.
- [25] Q. L. Wei, Z. Y. Jiang, S. S. Tan, Q. D. Li, L. Huang, M. Y. Yan, L. Zhou, Q. Y. An, L. Q. Mai, *ACS Appl. Mater. Interfaces* **2015**, *7*, 18211–18217.
- [26] G. A. Kallawar, B. A. Bhanvase, *Handbook of Nanomaterials for Wastewater Treatment*, Elsevier, **2021**, 699–737.
- [27] V. S. Rangasamy, S. Thayumanasundaram, J. P. Locquet, J. W. Seo, *Ionics* **2017**, *23*, 645–653.
- [28] V. K. Kumar, S. Ghosh, S. Biswas, S. K. Martha, *J. Electrochem. Soc.* **2021**, *168*, 030512.
- [29] K. Shanmuganathan, C. J. Ellison, in *Polymer Green Flame Retardants* (Eds: C. D. Papaspyrides, P. Kiliaris), Amsterdam: Elsevier, **2014**, 675–707.
- [30] Q. J. Mao, R. Gao, Q. Y. Li, D. Ning, D. Zhou, *Chem. Eng. J.* **2020**, *382*, 122978.
- [31] C. Delmas, C. Fouassier, P. Hagenmuller, *Physica B+C* **1980**, *99*, 81–85.
- [32] C. Delmas, J. Braconnier, C. Fouassier, P. Hagenmuller, *Solid State Ionics* **1981**, *3–4*, 165–169.
- [33] C. Peng, J. Liu, *Inorg. Chem. Indus.* **2023**, *55*, 1.
- [34] J. Xiong, L. He, Z. Zhao, *Desalination* **2022**, *535*, 115822.
- [35] F. Tournadre, L. Croguennec, P. Willmann, C. Delmas, *J. Solid State Chem.* **2004**, *177*, 2803–2809.
- [36] Z. Lu, J. R. Dahn, *J. Electrochem. Soc.* **2001**, *148*, A1225.
- [37] S. Komaba, N. Yabuuchi, *Inorg. Chem.* **2012**, *510*, 6211–6220.
- [38] J. Jiang, H. C. He, C. Cheng, T. Yan, X. Xia, M. Ding, L. He, T. S. Chan, L. Zhang, *ACS Appl. Energy Mater.* **2022**, *5*, 1252–1261.
- [39] J. Feng, S. H. Luo, J. Wang, P. Li, S. Yan, J. Li, P. Hou, Q. Wang, Y. Zhang, X. Liu, *ACS Sustain. Chem. Eng.* **2022**, *10*, 4994–5004.
- [40] S. Tao, W. Zhou, D. Wu, Z. Wang, B. Qian, W. Chu, A. Marcelli, L. Song, *J. Mater. Sci. Technol.* **2021**, *74*, 230–236.
- [41] T. Yuan, S. Li, Y. Sun, J. Wang, A. Chen, Q. Zheng, Y. Zhang, L. Chen, G. Nam, H. Che, J. Yang, S. Zheng, Z. Ma, M. Liu, *ACS Nano* **2022**, *16*, 18058–18070.
- [42] Y. Y. Xie, H. Wang, G. L. Xu, J. J. Wang, H. P. Sheng, Z. H. Chen, Y. Ren, C. J. Sun, J. G. Wen, J. Wang, D. J. Miller, J. Lu, K. Amine, Z. F. Ma, *Adv. Energy Mater.* **2016**, *6*, 1601306.
- [43] D. D. Yuan, Y. X. Wang, Y. L. Cao, X. P. Ai, H. X. Yang, *ACS Appl. Mater. Interfaces* **2015**, *7*, 8585–91.
- [44] Y. Zhang, M. M. Wu, W. Teng, J. W. Ma, R. Y. Zhang, Y. H. Huang, *ACS Appl. Mater. Interfaces* **2020**, *12*, 15220–15227.
- [45] G. Wan, Y. Chen, B. Peng, L. Yu, X. Ma, N. Ahmad, G. Zhang, *Battery Energy* **2023**, *2*, 20230022.
- [46] J. Wang, Z. Zhou, Y. Li, M. Li, F. Wang, Q. Yao, Z. Wang, H. Zhou, *J. Alloys Compd.* **2019**, *792*, 1054–1060.
- [47] Y. Lin, Q. Liu, Y. Liu, *J. Alloys Compounds* **2023**, *968*, 171808.
- [48] L. Xue, J. Z. Wang, Y. X. Teng, J. Lu, S. Bao, *Mater. Lett.* **2021**, *303*, 130507.
- [49] Y. S. Shi, S. Li, A. Gao, J. Y. Zheng, Q. H. Zhang, *ACS Appl. Mater. Interfaces* **2019**, *11*, 24122–24131.
- [50] Y. Zhang, C. C. Chen, G. W. Zhao, R. Y. Zhang, *ACS Sustain. Chem. Eng.* **2024**, *12*, 2729–2738.

- [51] H. V. Ramasamy, K. Kaliyappan, R. Thangavel, V. Aravindan, K. Kang, D. U. Kim, Y. I. Park, X. Sun, Y. S. Lee, *J. Mater. Chem.* **2017**, *5*, 13842–13842.
- [52] M. Z. Leng, J. Q. Bi, W. L. Wang, Z. Xing, W. K. Yan, X. C. Gao, J. Y. Wang, R. Liu, *Alloys Compounds* **2021**, *855*, 157533.
- [53] S. Bao, S. H. Luo, *Ceram. Int.* **2020**, *46*, 16080–16087.
- [54] F. P. Zhang, J. H. Liao, L. Xu, W. W. Wu, X. H. Wu, *ACS Appl. Mater. Interfaces* **2021**, *13*, 40695–40704.
- [55] Y. Q. Yang, R. B. Dang, K. Wu, Q. Li, N. Li, X. L. Xiao, Z. B. Hu, *Phys. Chem. C* **2020**, *124*, 1780–1787.
- [56] Y. Zhou, L. S. Li, Y. S. Wu, H. W. Xie, *Eur. J. Inorg. Chem.* **2023**, *26*, 202200685.
- [57] K. Tang, Y. Huang, X. Xie, S. Cao, L. Liu, M. Liu, Y. Huang, B. Chang, Z. Luo, X. Wang, *Chem. Eng. J.* **2020**, *384*, 123234.
- [58] M. L. Qin, C. Y. Yin, W. Xu, Y. Liu, J. Wen, B. Shen, W. Wang, W. Liu, *Trans. Nonferr. Met. Soc. China* **2021**, *31*, 2074–2080.
- [59] Y. N. Zhou, P. F. Wang, Y. B. Niu, Q. Li, X. Yu, Y. Yin, S. Xu, Y. Guo, *Nano Energy* **2019**, *55*, 143–150.
- [60] P. Zhang, G. H. Zhang, Y. K. Liu, Y. X. Fan, X. Y. Shi, Y. M. Dai, S. W. Gong, J. R. Hou, J. W. Ma, Y. H. Huang, R. Y. Zhang, *J. Colloid Interface Sci.* **2024**, *654*, 1405–1416.
- [61] X. Hu, H. Guo, J. Gao, Z. Liu, X. Ma, Y. Ge, Z. Wen, X. Jiao, K. Sun, D. Chen, *ACS Appl. Energy Mater.* **2024**, *7*, 460–468.
- [62] M. Kalapsazova, G. F. Ortiz, J. L. Tirado, O. Dolotko, E. Zhecheva, D. Nihtanova, L. Mihaylov, R. Stoyanova, *Chempluschem* **2015**, *80*, 1642–1656.
- [63] S. Y. Zhang, Y. J. Guo, Y. N. Zhou, X. D. Zhang, Y. B. Niu, E. H. Wang, L. B. Huang, P. F. An, J. Zhang, X. A. Yang, Y. X. Yin, S. L. Xu, Y. G. Guo, *Small* **2021**, *17*, 2007236.
- [64] A. Ramesh, A. Tripathi, M. Bosman, S. Xi, P. Balaya, *J. Electroanal. Chem.* **2023**, *932*, 117222.
- [65] M. H. Han, N. Sharma, E. Gonzalo, J. C. Pramudita, H. E. A. Brand, J. M. L. del Amo, T. Rojo, *J. Mater. Chem. A* **2016**, *4*, 18963–18975.
- [66] T. Yuan, Y. Y. Sun, S. Q. Li, H. Y. Che, Q. F. Zheng, Y. J. Ni, Y. X. Zhang, J. Zou, X. X. Zang, S. H. Wei, Y. P. Pang, S. X. Xia, S. Y. Zheng, L. W. Chen, Z. F. Ma, *Nano Res.* **2023**, *16*, 6890–6902.
- [67] Z. Cai, S. Wang, M. Tao, Q. Li, H. Mei, Z. Ahsan, Y. Ma, Z. Yu, G. Song, W. Yang, C. Wen, T. Yi, *J. Energy Storage* **2023**, *74*, 109391.
- [68] Y. Zhang, M. M. Wu, J. W. Ma, G. F. Wei, Y. Ling, R. Y. Zhang, Y. H. Huang, *ACS Central Sci.* **2020**, *6*, 232–240.
- [69] D. Yuan, X. Liang, L. Wu, Y. Cao, X. Ai, J. Feng, H. Yang, *Adv. Mater.* **2014**, *26*, 6301–6.
- [70] D. S. Bhange, G. Ali, D. H. Kim, D. A. Anang, T. J. Shin, M. G. Kim, Y. M. Kang, K. Y. Chung, K. W. Nam, *J. Mater. Chem. A* **2017**, *5*, 1300–1310.
- [71] H. Ya, *Small Methods* **2023**, *7*, 1601306.
- [72] P. F. Wang, M. Y. Weng, Y. Xiao, Z. X. Hu, Q. H. Li, M. Li, Y. D. Wang, X. Chen, X. N. Yang, Y. R. Wen, Y. X. Yin, X. Q. Yu, Y. G. Xiao, J. X. Zheng, L. J. Wan, F. Pan, Y. G. Guo, *Adv. Mater.* **2019**, *31*, 1903483.
- [73] E. Zemlyanushin, K. Pfeifer, A. Sarapulova, M. Etter, H. Ehrenberg, S. Dsoke, *Energies* **2020**, *13*, 6498.
- [74] Y. Liu, Y. H. Zhang, J. Ma, J. Zhao, X. Li, G. Cui, *Chem. Mater.* **2024**, *36*, 54–73.
- [75] J. Do, I. Kim, H. Kim, Y. Jung, *Energy Storage Mater.* **2020**, *25*, 62–69.
- [76] L. Q. Mu, X. Feng, R. Kou, Y. Zhang, H. Guo, C. X. Tian, C. J. Sun, X. W. Du, D. Nordlund, *Adv. Energy Mater.* **2018**, *8*, 1801975.
- [77] H. C. Ji, J. J. Zhai, G. J. Chen, X. Qiu, H. Fang, T. E. Zhang, Z. Y. Huang, W. G. Zhao, Z. H. Wang, M. H. Chu, R. Wang, C. Q. Wang, R. Li, W. Zeng, X. W. Wang, Y. G. Xiao, *Adv. Funct. Mater.* **2022**, *32*, 2109319.
- [78] Y. Sun, P. Zhou, S. Liu, Z. Zhao, Y. Pan, X. Shen, X. Wu, J. Zhao, *J. Energy Chem.* **2024**, *88*, 603–611.
- [79] T. Y. Yu, Y. K. Sun, *J. Mater. Chem. A* **2022**, *10*, 23639–23648.
- [80] X. H. Hu, Y. R. Wang, Y. Qiu, X. Yu, Q. H. Shi, Y. M. Liu, W. L. Feng, Y. F. Zhao, *Chemistry* **2024**, *19*, e202300960.
- [81] J. J. Fan, P. Dai, C. G. Shi, Y. F. Wen, C. X. Luo, J. Yang, C. Song, L. Huang, S. G. Sun, *Adv. Funct. Mater.* **2021**, *31*, 2010500.
- [82] L. Gao, J. Chen, Q. Chen, X. Kong, *Sci. Adv.* **2022**, *8*, eabm4606.

Manuscript received: July 15, 2024

Revised manuscript received: September 26, 2024

Accepted manuscript online: September 29, 2024

Version of record online: November 7, 2024